The global importance of metazoans to the biological carbon pump

Jérôme Pinti[1,2], Tim DeVries[3,4], Tommy Norin[1], Camila Serra-Pompei[1,5], Roland Proud[6], David A. Siegel[3,4], Thomas Kiørboe[1], Colleen M. Petrik [7,8], Ken H. Andersen [1], Andrew S. Brierley[6], André W. Visser[1]

[1]VKR Centre for Ocean Life, Technical University of Denmark, 2800 Kongens Lyngby, Denmark

[2] College of Earth, Ocean, and Environment, University of Delaware, Lewes, DE 19958, USA

[3] Department of Geography, University of California, Santa Barbara, CA 93106, USA

[4] Earth Research Institute, University of California, Santa Barbara, CA 93106, USA

[5] Department of Earth, Atmospheric and Planetary Sciences, Massachusetts Institute of Technology, Cambridge, MA 02139, USA

[6] Pelagic Ecology Research Group, School of Biology, Gatty Marine Laboratory, Scottish Oceans Institute, University of St Andrews, St Andrews, Fife KY16 8LB, UK

[7] Department of Oceanography, Texas A&M University, 3146 TAMU, USA

[8] Scripps Institution of Oceanography, University of California San Diego, La Jolla, CA 92107, USA

Abstract

The daily vertical migrations of fish and other metazoans actively transport organic carbon from the ocean surface to depth, contributing to the biological carbon pump. An important but unanswered question is whether fish play a significant role in the biological carbon pump relative to other organisms, both in terms of carbon export and sequestration. Here, we use a game-theoretic food-web model that simulates diel vertical migrations to estimate global carbon fluxes and sequestration by fish and zooplankton due to respiration, fecal pellets, and deadfalls. Despite uncertainties due to poorly constrained biomass estimates of some functional groups, a robust result of this model is that fish play a major role in the biological carbon pump. Our model estimates that open-ocean metazoans inject ∼3.1 (range 1.5 - 4.7) PgC/yr of a total of ∼10 PgC/yr into the ocean's interior. Fish are further responsible for 47% (25-65%) of the oceanic carbon sequestration mediated by metazoans. This essential ecosystem service provided by fishes could be at risk from unregulated fishing in the high seas.

Keywords— Diel Vertical Migrations, Food-webs, Game theory, Biological carbon pump, Carbon sequestration, Mesopelagic fish

Introduction

Many marine organisms – from zooplankton to fish – perform diel vertical migrations (DVM) (*1*, *2*), as they seek to both access food and avoid predators. Small planktivorous organisms feed close to the surface at night, and migrate to depth during daytime to reduce their predation risk from visual predators (*3*, *4*). In turn, higher trophic levels organise their vertical migrations to take advantage of their migrating prey while themselves avoiding predators. DVM within a marine pelagic community is therefore the product of a co-adaptive "game" where many animals seek to optimize their migration patterns relative to the migration patterns of their respective prey, predators and conspecifics (*5*–*7*).

These interacting DVM patterns govern trophic interactions (*8*) and affect global biogeochemical cycles (*9*). Migrating organisms transport carbon obtained through feeding at the surface to depth where it is released through respiration and excretion. This process, termed the active biological pump (or migrant pump), is highly efficient at sequestering carbon, because it injects carbon directly at depth and bypasses the remineralization experienced by passively sinking particles in the upper ocean (*10*). The biological pump is one of the ocean's key ecosystem services, as it mediates the draw-down of atmospheric carbon dioxide by transporting surface carbon to the ocean's deeper layers (*11*), where it can be sequestered for time scales ranging from years to centuries (*12*).

Several studies have explored the effects of DVM on carbon export (*13*–*15*), but have mainly focused on export mediated by zooplankton (*13*, *15*–*18*). Recent biogeochemical models estimate that active carbon fluxes at the base of the euphotic zone (our reference depth for export, unless otherwise stated) mediated by migrating organisms range between 1 and 30 $\mathrm{mgCm^{-2}day^{-1}}$, corresponding to 14-18% of the local passive sinking flux (*13*, *14*). However, these studies did not assess the carbon sequestration potential of these processes. Carbon sequestration represents the excess dissolved inorganic carbon (DIC) held in the oceans due to biological processes, and is an important measure to report in addition to carbon export (the rate of carbon being brought below the euphotic zone, either actively or by passive sinking), as the total amount of DIC held by the ocean determines the atmospheric CO_2 concentration (*9*).

How fish contribute to the biological carbon pump is currently poorly resolved (*19*, *20*). In particular, the contribution of mesopelagic fish is potentially of great importance, in part because of their high biomass, which has recently been estimated to be significantly higher than that of epipelagic fish (*21*, *22*). With biomass estimates ranging from 1.8 to 16 gigatonnes, mesopelagic fish harbour a huge – but uncertain – potential for active carbon sequestration through their DVMs and their excretion of fast-sinking fecal pellets (*2*, *19*).

We use a pelagic food-web model to investigate the potential impact of different metazoan functional groups (zooplankton, fish, jellyfish) and pathways (respiration, fecal pellets, deadfalls, other losses) on global ocean carbon budgets. We specifically consider how groups and pathways directly inject respired and egested carbon at depth, and their contribution to ocean carbon sequestration. That is, we focus not solely on export flux (i.e. carbon that sinks or is transported below the euphotic zone as organic carbon) but rather on the conversion of organic carbon into DIC (dissolved inorganic carbon) in the oceans' interior – what we term carbon injection. The latter is what matters for carbon sequestration, as carbon exported can be ingested again by detritivorous animals and brought back to the surface, whereas DIC cannot. We use spatially resolved realistic estimates of global biomasses to compute the DVM patterns of the different populations – which accord well with *in situ* observations of vertical distribution biomass –, and use these global patterns to compute active carbon injection mediated by each group, from both respiration at depth and degradation of sinking fecal pellets and deadfalls by bacteria and detritivorous organisms. Finally, we

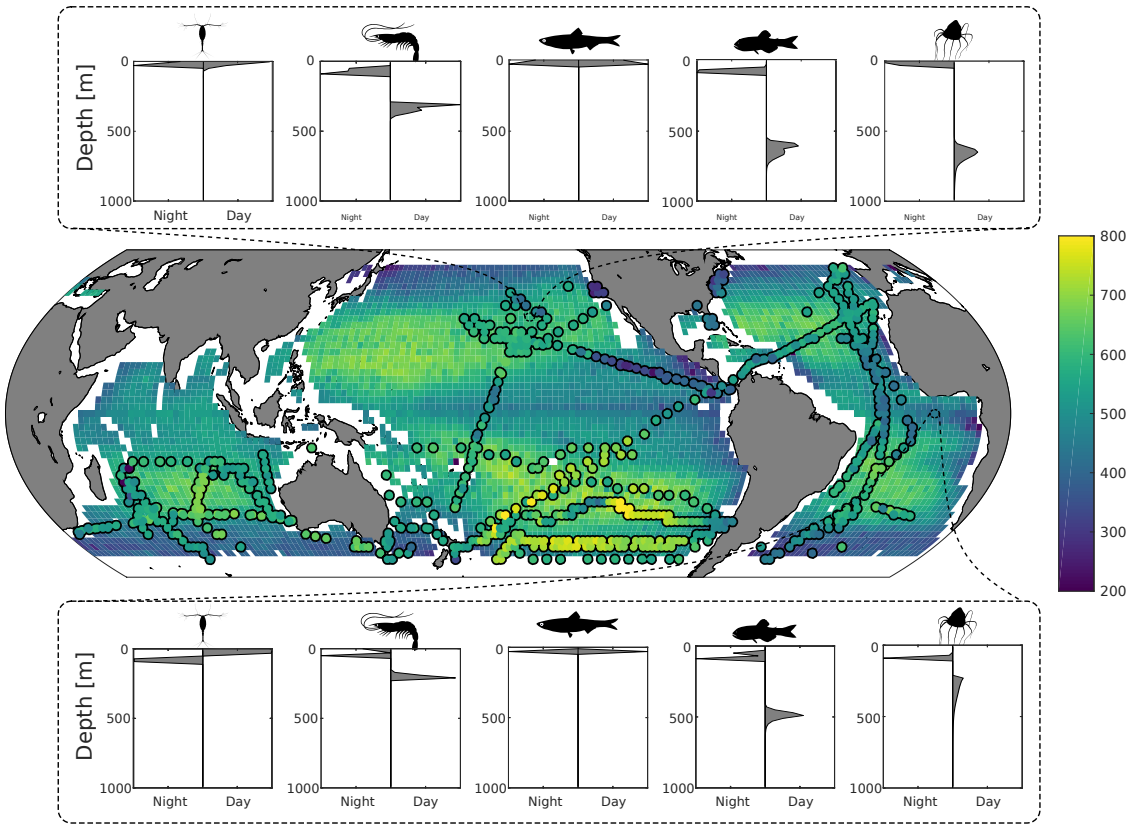

Figure 1: Top & bottom panels: predicted day and night depth distribution of meso-zooplankton, macro-zooplankton, forage fish, mesopelagic fish and jellyfish at 26°N 152°W and 7°S 0°E respectively. Middle panel: Predicted fish mean depth during daytime, weighted by biomass. Circles overlaid are the observed mean depths weighted by echo intensity recorded using 38 kHz echosounders (*2*, *25*, *26*).

combine our results with an ocean circulation inverse model (OCIM) (*23*, *24*) to estimate the total amount of carbon that is presently sequestered in the global ocean by the metazoan biological carbon pump, and the sequestration timescale of respired carbon.

We initialize the model with physiological parameters describing interactions between individuals and metabolic rates of the different functional groups, as well as the geographic distribution of physical parameters (light, temperature and oxygen levels) and the carbon biomass of different functional groups. We base our estimates on a reference simulation with the most probable parameter values, and provide a range of uncertainties for all reported fluxes, carbon sequestered estimates, and sequestration timescales, by varying the most uncertain parameters of the model by a fixed fraction of the reference value (typically between 50-150%, but mesopelagic fish biomass was varied between 20% and 200% of the reference value to account for the 10 fold range in biomass uncertainty). All reported uncertainties are the most extreme values obtained with the different sensitivity scenarios. These scenarios explore how the propagation of error plays out in this model by computing how all functions, behaviours, and carbon export and sequestration metrics respond to the change of one parameter.

Results

The predicted biomass-weighted mean depth (figure 1), taken as the model-predicted mean daytime depth of all fish weighted by biomass, is deeper in oceanic gyres (between 500-700 m deep), and shallower along the ocean margins and at the Equator (between 200-400 m). Predicted DVM patterns of the different functional groups (figure 1) can be compared to echosounder observations. Even though low frequency (e.g. 38 kHz) echosounder observations can be biased (*22*), they can be used as a proxy for estimating the mean depth of water-column communities (figure 1 and S7, (*2*, *25*, *26*)). Our simulations generally match echosounder observations: meso-zooplankton and forage fish remain close to the surface, whereas macro-zooplankton and mesopelagic fish (as well as jellyfish) perform vertical migrations everywhere (Figure 1). At temperate latitudes, our model predicts shallower migrations than observed, in particular in the Southern Ocean where seasonality can lead to large annual variations in DVM behaviour (*27*) coupled to zooplankton dormancy (*28*). The mechanistic formulation of the model and the global vertical distribution of

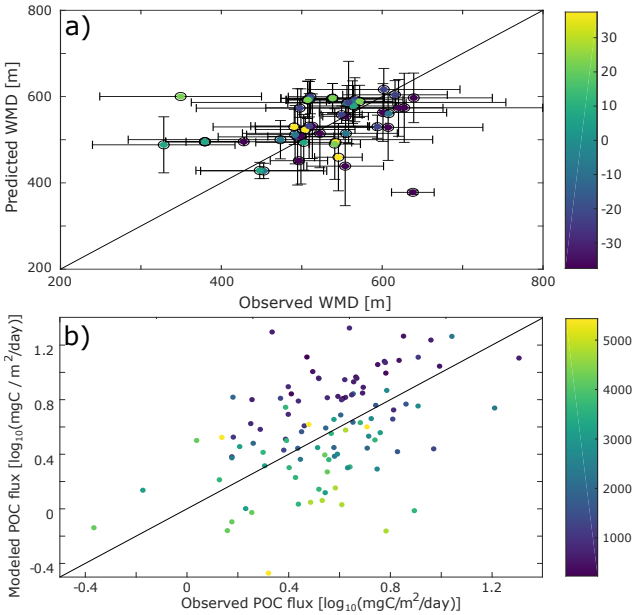

Figure 2: Comparison with data. a) Scatter plot of the differences between the observed and the model predicted depth of the deep scattering layer. b) Difference between the observed (from sediment traps data, (*29*)) and modeled POC flux. To decrease possible biases due to localized blooms, only fixed sediment traps deeper than 500m and with an annual coverage were selected for this comparison.

organisms enables us to compute the strengths of trophic couplings between different functional groups in the model (figure 3). We find the strongest coupling between mesopelagic fish (total biomass of 0.32 (0.06-0.64) PgC) and macro-zooplankton, with mesopelagic fish ingesting 1.3 (0.3-2.4) PgC of macro-zooplankton annually (the range of estimates refer to the most extreme values from the sensitivity analysis). Deadfalls and fecal pellets produced by metazoans in the euphotic zone contribute to a sinking flux of 1.0 (0.6-1.5) PgC yr^{-1} at the base of the euphotic zone (see figure 4 for local estimates). Additionally, 0.4 (0.2-0.7) PgC yr^{-1} of fecal pellets and 0.1 (0.1-0.3) PgC yr^{-1} of deadfalls are produced below the euphotic zone by metazoans, which also respire 1.1 PgC yr^{-1} (0.6 -1.7) PgC yr^{-1} through basal respiration and 0.4 (0.1-0.8) PgC yr^{-1} through other losses below the euphotic zone globally (see figures S11 and S12 for local estimates). Table 1 provides a summary of carbon injection rates due to the different pathways – basal respiration, fecal pellets, deadfalls, and other losses – for all functional groups.

Assuming that the system is at steady state, we can estimate the contributions of the different functional groups

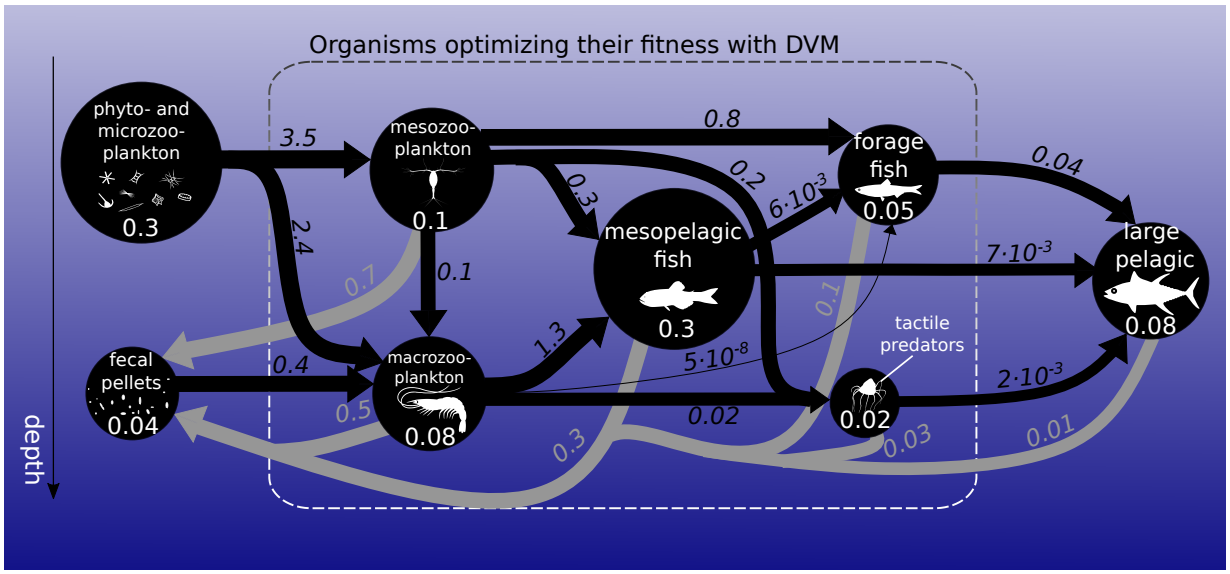

Figure 3: Biomass (circles) and fluxes (arrows) in the food-web integrated over the global ocean. Biomasses are in PgC (white numbers). Black arrows represent ingestion while grey arrows represent fecal pellet excretion in PgC yr^{-1}. Arrow widths and circle diameters are proportional to the logarithm of the fluxes and biomasses they represent. Respiration losses are not represented here. The dashed box surrounds the functional groups that optimize their day and night vertical distribution with DVM.

to carbon sequestration, as well as the corresponding residence times of respired carbon (figure 4 and table 1). Mesopelagic fish are the most important contributors to carbon sequestration with a total of 278 (53-708) PgC sequestered, followed by zooplankton (meso- and macro-zooplankton contribute 118 (37-266) and 230 (114-379) PgC respectively), forage fish (74 (34-113) PgC), and jellyfish (69 (28-122) PgC). Carbon sequestered via the fecal pellets pathway resides in the ocean longer than carbon sequestered via respiration (374 (178-635) years vs. 66 (44-77) years for all functional groups, table 1). In addition, carbon sequestered via degradation of fast-sinking fish fecal pellets or carcasses is stored on much longer time scales (up to 968 (757-1055) years for forage fish carcasses, and more than a thousand years for jellyfish and large pelagic fish carcasses) than carbon sequestered via degradation of slower-sinking fecal pellets such as meso-zooplankton (141 (43-360) years). While zooplankton produce the largest carbon fluxes globally, carbon injected via fish respiration or degradation of detritus originating from fish is stored more efficiently in the ocean's interior – all because larger organisms tend to remain deeper and because they produce larger particles that sink faster and thus escape remineralization in the upper parts of the water columns.

On a regional level, the absolute magnitude of carbon injected by metazoans below the euphotic zone varies significantly, from less than 10 to around 120 mgC m^{-2} day^{-1} (figure 4a). Subtropical gyres have the lowest injection, followed by the tropics, the Southern Ocean, the North Atlantic and North Pacific. The relative contribution of mesopelagic fish varies per geographic zone (figure S10), consistent with previous observations (*19*, *20*). Mesopelagic fish dominate carbon sequestration via the respiration pathway (more than 70% (34-82%) of the total) due to their deep daytime residence depths (figure 1).

Some aspects of our predictions can be compared to independent observations or constraints. We already commented on the DVM predictions. Our predictions of sinking particle fluxes can be compared to observations from sediment traps (figure 2b). While there are large differences between data and observations for some locations (up to

15 mgC m^{-2} day^{-1}), the predicted fluxes are of the same order of magnitude as those observed. There is no global or regional bias in these differences (figure S9) and the depth bias in modeled vs. observed sediment trap flux is consistent with biases usually witnessed for this type of data (*30*). Another comparison is the constraint on carbon sequestration provided by apparent oxygen utilization (AOU). The total respired carbon sequestration cannot exceed the amount implied by AOU given the stoichiometric relationship between oxygen consumption and dissolved inorganic carbon (DIC) production during respiration. Our carbon sequestration values are consistent with the AOU constraint, as they are well below those expected from World Ocean Atlas AOU estimates (*31*, figure S13). Predicted global ocean carbon sequestration constrained by World Ocean Atlas AOU data is 1770 PgC across the global ocean, while a recent study taking into account variations in the concentration of oxygen subducted into the interior ocean (*32*) estimated that the interior ocean stores 1300 ($\pm$ 230) PgC (compared to our estimate of 785 (417-1253) PgC for metazoans). The difference arises because we do not consider all export pathways (e.g. phytoplankton and aggregate sinkings), and that our spatial coverage accounts for only 63% of the global ocean (no coastal areas nor latitudes higher than $\pm 45°$). Our simulated AOU has a deeper maximum than the observed AOU because we resolve processes with faster sinking speed, whereas remaining processes (e.g. remineralization of DOC, aggregates and small fecal pellets from micro-zooplankton) would be concentrated in the upper oceans. Overall, our predictions of DVM, fluxes at depth, and AOU are compatible with available independent observations.

Because the large number of parameters and high computational cost of each simulation prohibit an exhaustive sensitivity analysis, we focused model sensitivity to nine poorly-constrained parameters: bacterial degradation rate, fecal pellet sinking speed, biomass of all functional groups, biomass of mesopelagic fish only, assimilation efficiencies, assimilation efficiency for detritus only, swimming speeds of all organisms, swimming speeds of mesopelagic fish only, and reference and maximum temperatures for all temperature-dependent rates. These parameters are anticipated to be those to which carbon injection and sequestration are most sensitive. Overall, the DVM patterns observed are robust (figure S14). Carbon injected and sequestered vary significantly between sensitivity scenarios, but are mostly of the same order as the ranges of the parameter variations (table S2-S22). This highlights the need to understand better mid-water animal ecology and to refine pelagic biomass data estimates, in order to constrain these parameters more. In addition, we ran a more detailed Monte-Carlo sensitivity analysis for five different ecoregions (subtropical gyres, tropical area, North Pacific, North Atlantic and Southern Ocean). This analysis confirms that the behaviour of organisms and passive and active injections are fairly robust to changes in parameter values (figures S16-S20). Respiration due to other losses, and to a lesser degree the sinking flux below the euphotic zone, is more sensitive to small changes in parameters than basal respiration and the production of detritus (fecal pellets or carcasses) below the euphotic zone. The sensitivity to changes in parameter values was similar within ocean ecoregions (figures S16-S20).

Discussion

Our results demonstrate that, despite large uncertainties, fish play a much more important role in the global carbon cycle than previously assumed – a hypothesis suggested by local estimates (*19*, *33*, *34*) and supported by an analysis of observed data in a recent review (*20*). Our model is not built on observations of DVM or carbon flux, but on fundamental mechanistic principles defining the interactions between individuals within different functional groups. These interactions lead to realistic vertical migration patterns and carbon fluxes that are coupled to a global ocean

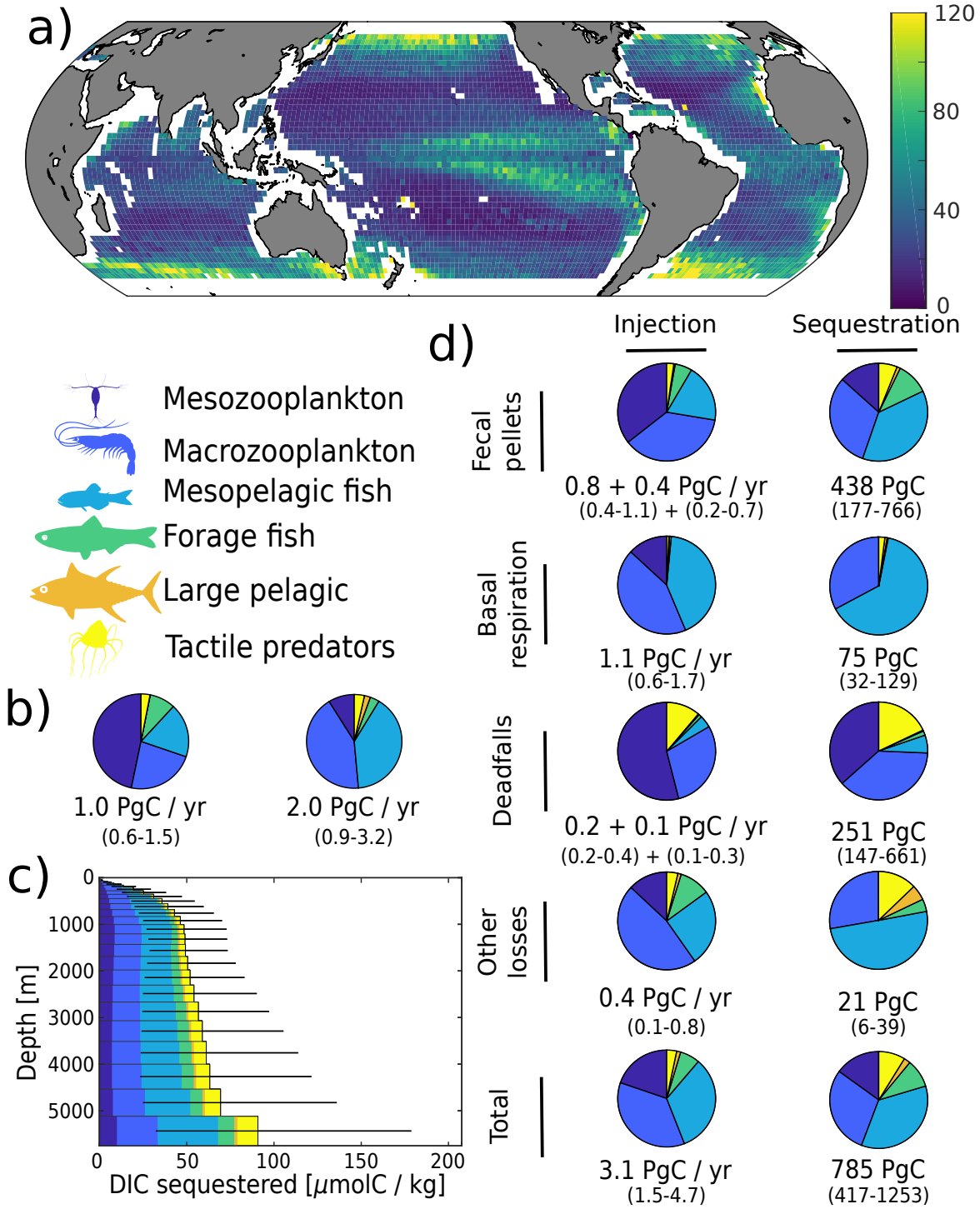

Figure 4: Simulated carbon injection and sequestration by metazoans. a) Simulated injection below the euphotic zone (in mgC m^{-2} day^{-1}). b) Relative contribution of the simulated functional groups to injection below the euphotic zone. Left panel corresponds to the degradation of organic carbon that was produced in the euphotic zone and subsequently sank below the euphotic zone, right panel corresponds to the degradation of organic carbon that was injected by metazoans directly below the euphotic zone. c) Globally averaged concentration of DIC according to the depth at which it is sequestered. d) Relative contribution of the functional groups to injection and sequestration (left and right column respectively) via the different pathways. For fecal pellets and carcass degradation, the first flux value corresponds to the degradation of organic carbon that was produced in the euphotic zone and subsequently sank below the euphotic zone, while the second corresponds to the degradation of organic carbon that was injected by metazoans directly below the euphotic zone. For basal respiration and other losses, only the direct injection below the euphotic zone is reported as there is no sinking flux for these pathways.

Table 1: Total injection, corresponding sequestration, and sequestration time for the different pathways considered in the model. Respiration pathway corresponds to animal respiration, fecal pellets pathway to bacterial respiration of metazoan fecal pellets, deadfalls to natural mortality, and other losses to all other losses. The range is obtained from the different scenarios of the sensitivity analysis, reported in section S7.1.

Organism	Respiration pathway			Fecal pellets pathway			Deadfalls pathway			Other losses			Total		
	Injection [PgC yr^{-1}]	Sequestr. [PgC]	Sequestr. time [yr]	Injection [PgC yr^{-1}]	Sequestr. [PgC]	Sequestr. time [yr]	Injection [PgC yr^{-1}]	Sequestr. [PgC]	Sequestr. time [yr]	Injection [PgC yr^{-1}]	Sequestr. [PgC]	Sequestr. time [yr]	Injection [PgC yr^{-1}]	Sequestr. [PgC]	Sequestr. time [yr]
Meso zoopl.	0.1	0.5	5	0.4	52	141	0.2	66	414	4e-03	0.02	4	0.6	118	185
	(0.04 - 0.2)	(0.1 - 1.3)	(2-9)	(0.2 - 0.6)	(12 - 138)	(43-360)	(0.1 - 0.2)	(25 - 127)	(177-749)	(0 - 4e-2)*	(0 - 0.3)*	(1-7)	(0.3 - 1.0)	(37 - 266)	(70-408)
Macro zoopl.	0.5	20	39	0.4	118	297	0.1	89	785	0.1	3	33	1.1	230	206
	(0.2 - 0.8)	(10 - 30)	(34-40)	(0.2 - 0.6)	(41 - 254)	(115-617)	(0.1 - 0.2)	(43 - 123)	(488-972)	(0 - 0.7)*	(0 - 22)*	(31-35)	(0.4 - 1.7)	(114 - 379)	(112-347)
Meso-pelagic	0.5	54	103	0.3	163	599	6e-02	49	851	0.2	11	63	1.0	278	270
	(0.1 - 1.0)	(11 - 107)	(101-130)	(0.1 - 0.5)	(34 - 317)	(271-896)	(8e-3 - 0.5)	(7 - 456)	(622-984)	(0 - 0.3)*	(0 - 26)*	(50-95)	(0.2 - 2.0)	(53 - 708)	(162-504)
Forage fish	3e-03	0.04	12	0.1	69	725	4e-03	4	968	0.1	0.5	10	0.2	74	475
	(1e-3 - 6e-3)	(0.01 - 0.09)	(6-28)	(0.04 - 0.1)	(30 - 107)	(415-909)	(2e-3 - 6e-3)	(2 - 6)	(757-1055)	(0.03 - 0.1)	(0.1 - 1.1)	(4-17)	(0.1 - 0.2)	(34 - 113)	(262-555)
Large pelagic	3e-03	0.4	156	0.01	12	987	9e-04	1	1003	0.03	4	154	0.04	17	407
	(1e-3 - 4e-3)	(0.2 - 0.6)	(155-157)	(0.03 - 0.04)	(4 - 30)	(878-1036)	(5e-4 - 1e-3)	(0.4 - 1)	(956-1021)	(0.01 - 0.07)	(1 - 10)	(145-158)	(0.01 - 0.1)	(5 - 41)	(339-475)
Jellyfish	1e-02	1	113	0.03	24	829	0.04	41	1018	0.03	2	67	0.1	69	642
	(4e-3 - 2e-2)	(0.5 - 2)	(95-142)	(0.01 - 0.06)	(7 - 53)	(501-1005)	(0.02 - 0.06)	(21 - 62)	(854-1084)	(2e-3 - 0.07)	(0.1 - 6)	(50-105)	(0.04 - 0.2)	(28 - 122)	(492-871)
Total	**1.1**	**75**	**66**	**1.2**	**438**	**374**	**0.4**	**251**	**666**	**0.4**	**21**	**54**	**3.1**	**785**	**255**
	(0.6 - 1.7)	**(32 - 129)**	**(44-77)**	**(0.5 - 1.8)**	**(177 - 766)**	**(178-635)**	**(0.3 - 0.8)**	**(147 - 661)**	**(428-891)**	**(0.1 - 0.8)**	**(6 - 39)**	**(37-64)**	**(1.5 - 4.7)**	**(417-1253)**	**(147-395)**

*Here, the lowest injection and sequestration value obtained for other losses was negative (and was truncated to 0), meaning that some parameter settings (very high mesopelagic fish biomass) are not compatible with a viable micro- and macro-zooplankton population.

circulation model to assess global carbon sequestration. In our model, fish (including mesopelagic fish, forage fish, and large predators) account for 40% (14-60%) of the carbon injected by metazoans below the euphotic zone. Assuming a global carbon export due to all processes (i.e. including phytoplankton and microzooplankton) of around 9-10 PgC yr^{-1} (*35–38*), this suggests that fish are responsible for 12% (4-23%) of total export. This figure is in line with a recent literature review of local studies that estimated that fish were responsible for around 16% (± 13%) of carbon flux out of the euphotic zone (*20*). More important, our analysis suggests that fish are responsible for 47% (25-65%) of simulated carbon sequestration by metazoans (table 1). The large influence of fish on carbon sequestration (relative to injection) is due to the deep migration depths of mesopelagic fish, and the production of large fast-sinking fecal pellets, both of which lead to long sequestration times for the resulting respired DIC. While these first global mechanistic estimates of DVM patterns and fish carbon sequestration are subject to uncertainty, they provide a baseline for future assessments and for evaluating the carbon sequestration impact of fishing.

Present global estimates of carbon export are 9-10 PgC yr^{-1} (*35–38*). Our model estimates a total carbon export of 2.0 (1.2-13.0) PgC yr^{-1} below the euphotic zone (table S1), mostly from macro-zooplankton and mesopelagic fish fecal pellets. The difference between the global estimate of 9-10 PgC yr^{-1} and our estimate is because our model does not include detrital aggregates derived from phytoplankton and unicellular organisms, estimated to account for an additional 1-2 PgC yr^{-1} (*38–40*), nor the sinking of fecal pellets and carcasses from microzooplankton, estimated to account for 3-4 PgC yr^{-1} (*38*). Further, our model does not include coastal areas (shallower than 500 m) nor latitudes higher than ±45°. Coastal areas were not included because our model is unsuited to shallow continental shelf regions, and high latitudes were not included because of their seasonality – although they can have important consequences for carbon export, through e.g. zooplankton dormancy (*41*). With the same spatial coverage as our model, the SIMPLE-TRIM carbon export model (a data-constrained model that estimates a global export flux of ∼9 PgC yr^{-1}, *37*) predicts a total export flux out of the euphotic zone of ∼6 PgC yr^{-1} consistent with the values provided above.

In addition to the passive sinking of fecal pellets and carcasses, our model also predicts carbon export by active diel vertical migration. Other modelling studies that have assessed the role of DVM on carbon export have relied on heuristics rather than mechanistic principles (*13*, *14*), and rarely considered functional groups separately to assess their relative importance (*13*). Their resulting estimates mostly align with ours. Aumont et al. (*14*) estimated that all migrating organisms export about 1.0 PgC yr^{-1} below 150 m (this depth is always deeper than the euphotic zone limit, so this result is hard to relate directly to ours), and Archibald et al. (*13*) found that zooplankton are responsible for the export of about 0.8 PgC yr^{-1} below the euphotic zone. Global carbon export measurements estimate that mesopelagic fish are responsible for a carbon flux of 1.5 ±1.2 PgC yr^{-1} (*20*), a figure in agreement with our simulated injection of 1.0 (0.2-2.0) PgC yr^{-1}. Note that here we are using carbon injection and not carbon export. Carbon injection is a more relevant metric when it comes to metazoan-driven carbon transport, as (organic) carbon exported can be uptaken again by detritivorous organisms, while carbon injected (in the form of dissolved inorganic carbon) cannot be reused by metazoans.

Our results are relatively robust, as a factor 2 change in the most sensitive parameter values leads to a factor 2 change in export. The relative importance of fish for carbon sequestration remains high throughout the sensitivity analysis. One of the most sensitive inputs is biomass, and global estimates are highly uncertain. For example, mesopelagic fish global biomass estimates vary between 20 and 200% of the reference estimate due to the uncertainty

in translating echosounder observations into biomass estimates (*22*). Gelatinous zooplankton estimates are still highly imprecise (*42*), but potentially of considerable importance. A recent study (*43*) estimated that gelatinous zooplankton were responsible for a global export of 1.6-5.2 PgC yr^{-1} below 100 m. Even though that study included coasts and high latitudes and had a fixed depth horizon, their estimate is still much higher than our estimate of a total injection of 0.1 (0.04-0.2) PgC yr^{-1} below the euphotic zone for jellyfish, perhaps because their study –unlike this one– included gelatinous zooplankton that can also feed on phytoplankton and micro-zooplankton.

An omitted functional group of this model is bathypelagic fish. These fish constantly live below ∼1000 m, potentially migrating daily between bathyal depths (up 4000 m deep) and the mesopelagic zone, taking up the lower rungs of Vinogradov's ladder (*44*). These organisms, feeding on mesopelagic fish (that can also, sometimes, migrate below 1000 m (*34*, *45*)), would tend to increase the time scales on which carbon is sequestered. The biomass of bathypelagic fish is, however, even less well known than the biomass of mesopelagic fish. Therefore, their potential contribution to global carbon sequestration is hard to assess. We can only conjecture that carbon sequestrated because of bathypelagic fish respiration and excretion would be sequestrated on very long time scales given the depths at which these organisms live. This consideration emphasizes further the importance of considering carbon injection and sequestration in addition to carbon export. While carbon export is an important metric, it only gives a partial idea of ocean carbon budgets. Carbon injection – the depth dependent biologically mediated source of DIC – is a more relevant metric that all biological pump studies should strive to estimate, whether focusing on the degradation of sinking POC (i.e. bacterial respiration) or respiration from vertical migrants.

As anthropogenic pressures increase, the last realm to remain relatively undisturbed by human activities is the deep sea. This may change because of commercial incentives to fish on the vast resource that mesopelagic fish represents (*46*). It has been suggested that 50% of the existing mesopelagic biomass can be sustainably extracted (*46*). However, fishing may have implications for carbon sequestration (*47*, *48*). Even by assuming that only 25% of their biomass is harvested annually, then to first order that would reduce their contribution by 25%, i.e., by 70 (13-177) PgC (which is equivalent to 257 (49-655) Pg CO_2). At € 80 per tonne of CO_2 (CO_2 European Emission Allowances, April 2022), the carbon off-set value of 25% of mesopelagic fish biomass would be € 20 (4-52) trillion. This estimate demonstrates that there is a trade-off between economic gain of developing mesopelagic fishing and the cost of the forgone carbon sequestration.

Methods

The behavioural part of our model is a 1D model depicting a pelagic community, from surface waters to mesopelagic depths (figure 3). The model resolves migrating functional groups: meso-zooplankton, macro-zooplankton, forage fish, large pelagic fish, jellyfish, and mesopelagic fish, as well as non-migrating resources of phytoplankton and micro-zooplankton. The biomass of all groups is fixed. The vertical distribution of phytoplankton depends on the mixed layer depth. Large pelagic fish are assumed to be uniformly distributed in the water column as they are proficient swimmers that are able to move up and down the water column several times a day Holland1992, Thygesen2016. This distribution also implies a uniform distribution of predation risk (depth effects aside) for prey, consistent with the fact that predators can relocate much faster than their prey. All other functional groups can move in the water column and our model computes the optimal day and night distribution of all organisms in the water column simultaneously.

Detritus is created by organisms (through fecal pellet production or by natural mortality), sinks, and gets degraded or ingested by macro zooplankton along the way.

An organism's optimal strategy (i.e. day and night positions) maximises its fitness given the position of all other organisms in the water column. As an individual selects a strategy, the fitness of its prey, predators and conspecifics also varies. Hence, the optimal strategy of all individuals is intrinsically linked to the optimal strategy of all other players. The optimal strategies for all individuals is attained at the Nash equilibrium Nash1951, where no individual can increase its fitness by changing its strategy. The Nash equilibrium is found using the replicator equation Hofbauer2003, Pinti2019, Pinti2019b. In short, the fraction of the population following a particular strategy grows proportionally to the fitness related to that strategy.

The fitness measure used is Gilliam's rule Houston1993, i.e. growth divided by mortality. In a steady environment, this is a valid approximation to life-time reproductive success as an organism that constantly optimises this measure will maximise its life-time reproductive success Sainmont2015. The fitness is calculated from simple trait-based mechanistic principles. In the water column, abiotic conditions (temperature, light levels, oxygen concentration) vary vertically, impacting vital rates and trophic interactions between organisms, in turn affecting the fitness of organisms. Light levels also vary between day and night, creating the possibility for organisms to perform DVM — if the optimal strategy is to change vertical position during day and night. Mixed layer depths vary spatially, impacting the distribution of phytoplankton.

The growth rate of organisms is the assimilation rate minus standard metabolic rate and migration cost. The mortality rate is the mortality due to predation plus a small background mortality. Predators and prey swim at a constant speed and encounter each other depending on the clearance rate of the predator (for visual predators, this varies vertically due to light attenuation in the water and between day and night). The probability of capture in each encounter event depends on the escape speed of prey and the attack speed of predators, both varying with the aerobic scope of the corresponding organism (which depends on the local oxygen and temperature conditions). The ingestion rate of each organism is modulated by a type II functional response, except for jellyfish that follow a type I functional response with no saturation at high prey concentrations Holling1959, Titelman2006. An ingested prey is then assimilated with a certain efficiency. The fraction not assimilated is egested as fecal pellets. Moreover, organisms dying of natural mortality (background mortality and not predation) sink as carcasses with a fast sinking velocity, bringing carbon to depths as carcasses get degraded by bacteria. All details, equations and parameters for fitness calculations are given in the supplementary material.

This 1D behavioural model is run at a global scale, informed by global biomass, temperature and oxygen levels estimates. Global biomass estimates of plankton are outputs of the COBALT model Stock2014,Stock2017, forage fish and large pelagic fish biomasses are outputs of the FEISTY model Petrik2019, and mesopelagic fish biomass is calculated from acoustic backscatter Proud2017, Proud2018. Environmental drivers (temperature, oxygen, light attenuation coefficient, and mixed layer depth) are taken from the World Ocean Atlas 2018 Locarnini2019,Garcia2019. Global inputs are pictured in figures S4 and S5.

Once the global behaviour of organisms is computed, we compute the amount of carbon respired, egested as fecal pellets, or sinking as carcasses for each functional group. This directly provides us with global carbon export and injection estimates. The animal respiration rates (basal respiration and other losses – an aggregate of all processes not accounted for in the model, such as specific dynamic action and reproduction) and bacterial respiration rates (due

to the degradation of fecal pellets and carcasses) are then used to compute the carbon sequestration by each pathway using a data-constrained steady-state ocean circulation inverse model [OCIM,][]DeVries2011,DeVries2014, Holzer2021, providing estimates of the amount of carbon sequestered in the oceans via the different pathways, assuming equilibrium conditions. Dividing the amount of carbon sequestered by the corresponding global injection yields the sequestration time of respired carbon, a measure of the time scale on which carbon is sequestered.

The source code (written in MATLAB) supporting this article has been uploaded as part of the supplementary material and is available at: `https://github.com/JeromeAqua/Global_contribution_fish`

Data, code and material

The source code (written in MATLAB) supporting this article has been uploaded as part of the supplementary material and is available at: `https://github.com/JeromeAqua/Global_contribution_fish`.

Acknowledgements

This work was supported by the Centre for Ocean Life, a VKR Centre of excellence funded by the Villum Foundation, and by the Gordon and Betty Moore Foundation (grant #5479). ASB and RP were funded in part through the EU BG3 project 'SUMMER' and BG8 project 'Mission Atlantic'. Collated echosounder data obtained from the BODC included observations made during the Atlantic Meridional Transect. The Atlantic Meridional Transect is funded by the UK Natural Environment Research Council through its National Capability Long-term Single Centre Science Programme, Climate Linked Atlantic Sector Science (grant number NE/R015953/1). This study contributes to the international IMBeR project and is contribution number 378 of the AMT programme.

Author contributions

JP designed the study with help from AWV and TK. RP, CMP, and ASB contributed biomass data. JP conducted the study with technical assistance from TDV, TN, CSP, DAS, TKA, KHA, and AWV. JP analysed results with help from TDV, DAS, CSP, TK, KHA, and AWV. JP wrote the manuscript with contributions from all authors. All authors approved the manuscript and agreed to be held personally accountable for their own contributions.

References

1. I. A. McLaren, *Journal of the Fisheries Research Board of Canada* **20**, 685–727, ISSN: 0015-296X (1963).
2. T. A. Klevjer *et al.*, *Scientific Reports* **6**, 19873 (Apr. 2016).
3. T. M. Zaret, S. Suffern, *Limnology and Oceanography* **21**, 804–813, ISSN: 00243590 (1976).
4. W. Lampert, *Archiv her Hydrobiologie, Beiheft Ergebnisse der Limnologie* **39**, 79–88, (`https://pure.mpg.de/pubman/faces/ViewItemOverviewPage.jsp?itemId=item%7B%5C_%7D1508686%20http://www.crcnetbase.com/doi/10.1081/E-EEE2-120046011`) (Dec. 1993).

5. D. M. Hugie, L. M. Dill, *Journal of Fish Biology* **45**, 151–169 (1994).

6. J. Pinti, A. W. Visser, *The American Naturalist* **193**, E000–E000, ISSN: 0003-0147, (https://www.journals.uchicago.edu/doi/10.1086/701041) (Dec. 2019).

7. J. Pinti, T. Kiørboe, U. H. Thygesen, A. W. Visser, *Proceedings of the Royal Society B: Biological Sciences* **286**, 20191645 (Sept. 2019).

8. K. Bandara, Ø. Varpe, L. Wijewardene, V. Tverberg, K. Eiane, *Biological Reviews* (2021).

9. K. O. Buesseler, P. W. Boyd, *Limnology and Oceanography* **54**, 1210–1232, ISSN: 00243590 (2009).

10. P. W. Boyd, H. Claustre, M. Levy, D. A. Siegel, T. Weber, *Nature* **568**, 327–335, ISSN: 14764687, (http://dx.doi.org/10.1038/s41586-019-1098-2) (2019).

11. P. G. Falkowski, R. T. Barber, V. Smetacek, *Science* **281**, 200–206, ISSN: 00368075 (1998).

12. T. DeVries, F. Primeau, C. Deutsch, *Geophysical Research Letters* **39**, 1–5, ISSN: 00948276 (2012).

13. K. M. Archibald, D. A. Siegel, S. C. Doney, *Global Biogeochemical Cycles* **33**, 181–199 (2019).

14. O. Aumont, O. Maury, S. Lefort, L. Bopp, *Global Biogeochemical Cycles* **32**, 1–22, ISSN: 19449224, (https://agupubs.onlinelibrary.wiley.com/doi/abs/10.1029/2018GB005886?af=R) (2018).

15. T. Gorgues, O. Aumont, L. Memery, *Geophysical Research Letters*, 2018GL081748, ISSN: 0094-8276, (https://onlinelibrary.wiley.com/doi/abs/10.1029/2018GL081748) (2019).

16. A. Longhurst, A. Bedo, W. Harrison, E. Head, D. Sameoto, *Deep Sea Research Part A. Oceanographic Research Papers* **37**, 685–694, ISSN: 01980149, (http://linkinghub.elsevier.com/retrieve/pii/019801499090098G) (Apr. 1990).

17. D. K. Steinberg *et al.*, *Deep Sea Research Part I* **47**, 137–158, ISSN: 09670637 (Jan. 2000).

18. A. N. Hansen, A. W. Visser, *Limnology and Oceanography* **61**, 701–710, ISSN: 19395590 (2016).

19. P. C. Davison, D. M. Checkley, J. A. Koslow, J. Barlow, *Progress in Oceanography* **116**, 14–30, ISSN: 00796611, (http://dx.doi.org/10.1016/j.pocean.2013.05.013) (2013).

20. G. K. Saba *et al.*, *Limnology and Oceanography*, 1–26 (2021).

21. X. Irigoien *et al.*, *Nature communications* **5**, 3271, ISSN: 20411723, (http://www.nature.com/doifinder/10.1038/ncomms4271) (Feb. 2014).

22. R. Proud, N. O. Handegard, R. J. Kloser, M. J. Cox, A. S. Brierley, *ICES Journal of Marine Science* **76**, ed. by D. Demer, 718–733, ISSN: 1054-3139, (https://academic.oup.com/icesjms/article/76/3/718/4978316) (May 2019).

23. T. DeVries, F. Primeau, *Journal of Physical Oceanography* **41**, 2381–2401, ISSN: 00223670 (2011).

24. T. DeVries, *Global Biogeochemical Cycles* **28**, 631–647, ISSN: 19449224 (2014).

25. IMOS, *IMOS BASOOP sub facility*, 2021, (2021; imos.org.au).

26. Polar Data Centre British Antarctic Survey, *Raw acoustic data collected by ship-borne EK60 echosounder in the Atlantic Ocean (AMT24, AMT25, AMT26, AMT29)*. (2020).

27. P. K. Prihartato, D. L. Aksnes, S. Kaartvedt, *Marine Ecology Progress Series* **521**, 189–200 (2015).

28. K. Bandara *et al.*, *Marine Ecology Progress Series* **555**, 49–64, ISSN: 01718630 (2016).

29. M. J. Lutz, K. Caldeira, R. B. Dunbar, M. J. Behrenfeld, *Journal of Geophysical Research: Oceans* **112**, ISSN: 21699291 (2007).

30. R. Schlitzer, R. Usbeck, G. Fischer, in *The South Atlantic in the Late Quaternary: Reconstruction of material budgets and current systems*, ed. by G. Wefer, S. Mulitza, V. Ratmeyer (Springer-Verlag, 2003), pp. 1–19, ISBN: 9783642189173.

31. H. Garcia *et al.*, "WORLD OCEAN ATLAS 2018 Volume 3: Dissolved Oxygen, Apparent Oxygen Utilization, and Dissolved Oxygen Saturation", tech. rep. (Silver Spring, MD, 2019), p. 38, (`https://www.nodc.noaa.gov/OC5/woa18/pubwoa18.html`).

32. B. R. Carter *et al.*, *Global Biogeochemical Cycles* **35**, ISSN: 19449224, (`https://doi.org/10.1029/2020GB006623`) (2021).

33. G. K. Saba, D. K. Steinberg, *Scientific Reports* **2**, 1–6, ISSN: 20452322 (2012).

34. J. M. Hudson, D. K. Steinberg, T. T. Sutton, J. E. Graves, R. J. Latour, *Deep-Sea Research Part I: Oceanographic Research Papers* **93**, 104–116, ISSN: 09670637, (`http://dx.doi.org/10.1016/j.dsr.2014.07.002`) (2014).

35. R. Schlitzer, *Deep-Sea Research Part II: Topical Studies in Oceanography* **49**, 1623–1644, ISSN: 09670645 (2002).

36. J. P. Dunne, R. A. Armstrong, A. Gnnadesikan, J. L. Sarmiento, *Global Biogeochemical Cycles* **19**, 1–16, ISSN: 08866236 (2005).

37. T. DeVries, T. Weber, *Global Biogeochemical Cycles* **31**, 535–555, ISSN: 19449224 (2017).

38. K. Bisson, D. A. Siegel, T. DeVries, *Frontiers in Marine Science* **7**, 1–15, ISSN: 22967745 (2020).

39. D. A. Siegel *et al.*, *Global Biogeochemical Cycles* **28**, 181–196, ISSN: 08866236, (`http://doi.wiley.com/10.1002/2014GB004853%20http://doi.wiley.com/10.1002/2013GB004743`) (Mar. 2014).

40. M. E. Nowicki, T. Devries, D. A. Siegel, *Global Biogeochemical Cycles* **36**, e2021GB007083 (2022).

41. S. H. Jónasdóttir, A. W. Visser, K. Richardson, M. R. Heath, *Proceedings of the National Academy of Sciences* **112**, 12122–12126, ISSN: 0027-8424, arXiv: `0812.0143v2`, (`http://www.pnas.org/lookup/doi/10.1073/pnas.1512110112`) (Sept. 2015).

42. C. H. Lucas *et al.*, *Global Ecology and Biogeography* **23**, 701–714, ISSN: 14668238 (2014).

43. J. Y. Luo *et al.*, *Global Biogeochemical Cycles* **34** (2020).

44. M. Vinogradov, *ICES reports* **18**, 114–120 (1962).

360 *45.* A. Ariza, J. C. Garijo, J. M. Landeira, F. Bordes, S. Hernández-León, *Progress in Oceanography* **134**,
361 330–342, ISSN: 00796611, (`http://dx.doi.org/10.1016/j.pocean.2015.03.003`) (2015).

362 *46.* M. A. St. John *et al.*, *Frontiers in Marine Science* **3**, 1–6, ISSN: 2296-7745 (2016).

363 *47.* G. Mariani *et al.*, *Science advances* **6**, 1–9, ISSN: 23752548 (2020).

364 *48.* D. Bianchi, D. A. Carozza, E. D. Galbraith, J. Guiet, T. DeVries, *Science Advances* **7**, ISSN: 23752548
365 (2021).